CFD ANALYSIS ON VERTICAL MOTION OF A FULL-SCALE FLOATING JETTY

AHMAD FITRIADHY* AND AMIRA ADAM

Faculty of Ocean Engineering Technology and Informatics, Universiti Malaysia Terengganu, 21030 Kuala Nerus, Terengganu, Malaysia.

Corresponding author: naoe.afit@gmail.com

Abstract: A floating jetty often experiences several vertical motions i.e., heave and pitch motion responses due to harsh environmental condition. This inherently makes discomfort to everyone during berthing on a floating; and even it potentially leads to loss of life due to falling down into the sea. A preliminary analysis using Computational Fluid Dynamics (CFD) simulation is necessary to be conducted to ensure user's safety. The CFD analysis focused on the interaction between wave motions and the floating jetty and its effects on the vertical motions. The vertical motions of floating jetty were quantified by the Response Amplitude Operators (RAO). Several effects due to variation of wavelength (λ/L) have been studied. The CFD results revealed that the lower wavelength ($\lambda/L < 2.25$) resulted in the increase of the heave and pitch motion amplitudes proportionally. However, the subsequent increase of wavelength ($2.25 > \lambda/L$) has given results to less heave and pitch motion amplitudes. In general, it is shown that the vertical motion characteristics of the floating jetty predominantly depend on wave properties.

Keywords: CFD, floating jetty, wavelength, heave, pitch.

Introduction

A serious coastal erosion along Tok Jembal's coastline areas has led to local massive natural destructions. In fact, this situation has caused excessively sediment transports and change the shoreline bathymetry along the coastline. As to overcome such a problem, the State Government of Terengganu has developed and installed successfully a breakwater. This preventive action may be taken as an ad-hock solution to reduce or eliminate a more undesirable devastation from happening in the future.

Despite the installation of the breakwater, the activities of loading and unloading of the fish catches by the fishermen were still unsafe due to waves pounding and changes in water-depths between low and high tides. Universiti Malaysia Terengganu has addressed the problem faced by the fishermen and come up with the beneficial solution through development and fabrication of a landing infrastructure facility known as "a floating jetty". This project is called as "community project" with funds were provided by Knowledge Transfer and Assimilation Grant (KTAG). This floating jetty is intended to be used by for about 40 members of the local fisherman community.

As seen in Figure 1, the current floating jetty has been designed and constructed of a multi-hulls model. This concept design leads to lower wave excitation forces and lower amplitude of the vertical motion responses i.e., heave and pitch motions as compared to the mono-hull model as written by (Davis & Holloway, 2007; Grigoropoulos *et al.,* 2003; Kim *et al., 2017)*. Meanwhile, these multi-hulls concept design is adopted from trimaran hull form model, which provides a better stability and the response amplitude motions based on its insignificant response at higher wave heading (Aribenchi, 2017; Luhulima *et al.,* 2014). Correspondingly, a further investigation of the floating jetty motion responses in the preliminary design of the floating jetty, to ensure safety to users during operation.
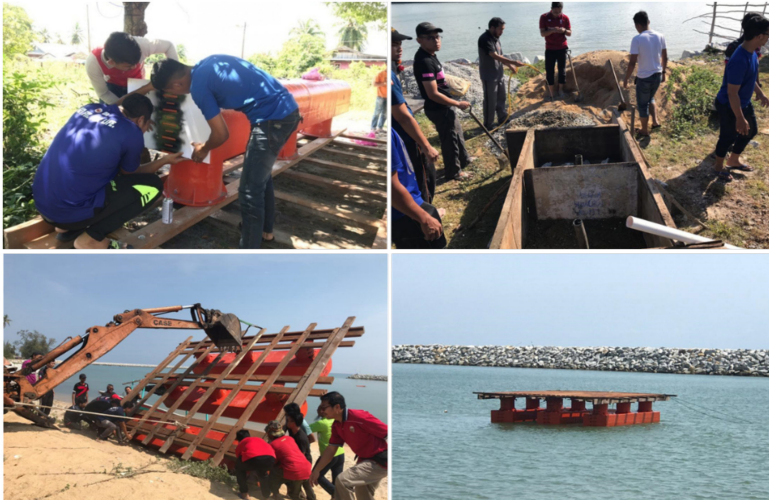
Figure 1: Floating jetty construction process

The paper presents Computational Fluid Dynamics (CFD) simulation to assess the vertical motions (heave and pitch) performance of the floating jetty in waves similar with (A. Fitriadhy *et al.,* 2017). The studies employ full-scale dimensions of the floating jetty to obtain the actual amplitudes of the vertical motion responses. Effects of various wavelengths (λ/L) have been taken into account in the CFD simulation. A commercial CFD software namely Flow-3D v11.2 is employed through application of unsteady Reynolds-Averaged Navier Stokes Equation (RANSE); which includes several techniques (TruVOF) to capture the free surface effect. The Response Amplitude Operator (RAO) of heave and pitch motion performances are then discussed.

Governing Equation

Two basic governing equations in accordance to the law conservation of mass and momentum as clearly expressed in Eqs. (1)-(4), were used. The current CFD simulation is based on the incompressible unsteady RANSE, which employs the volume of fluid (VOF).

Continuity and Momentum Equation

The general mass continuity equation presented in Eq. (1), for a moving object and the comparative VOF function transport equation; where the V_F is the fractional volume open to flow, ρ is the fluid density, R_{DIF} is a turbulent diffusion term, R_{SOR} is a mass source and A_x, A_y and A_z is the fractional area open to flow in x, y and z-direction, respectively (Manual, 2011).

The momentum theory also applies in three coordinates direction (*u, v, w*) that has been used in the motion equation as displayed in Eqs. (2)-(4).

$$V_F \frac{\partial \rho}{\partial t} + \frac{\partial}{\partial x}(\rho u A_x) + R \frac{\partial}{\partial y}(\rho v A_y) + \frac{\partial}{\partial z}(\rho \omega A_z) + \xi \frac{\rho u A_x}{x} = R_{DIF} + R_{SOR} \qquad (1)$$

$$\frac{\partial u}{\partial t} + \frac{1}{V_F}\left\{uA_x\frac{\partial u}{\partial x} + vA_yR\frac{\partial u}{\partial y} + uA_z\frac{\partial u}{\partial z}\right\} - \xi\frac{A_yv^2}{xV_F} = -\frac{1}{\rho}\frac{\partial p}{\partial x} + G_x + f_x - b_x -$$

$$\frac{R_{SOR}}{\rho V_F}(u - u_w - \delta u_s) \tag{2}$$

$$\frac{\partial v}{\partial t} + \frac{1}{V_F}\left\{uA_x\frac{\partial v}{\partial x} + vA_yR\frac{\partial v}{\partial y} + uA_z\frac{\partial v}{\partial z}\right\} + \xi\frac{A_yuv}{xV_F} = -\frac{1}{\rho}(R)\frac{\partial p}{\partial y} + G_y + f_y - b_y -$$

$$\frac{R_{SOR}}{\rho V_F}(v - v_w - \delta v_s) \tag{3}$$

$$\frac{\partial w}{\partial t} + \frac{1}{V_F}\left\{uA_x\frac{\partial w}{\partial x} + vA_yR\frac{\partial w}{\partial y} + uA_z\frac{\partial w}{\partial z}\right\}$$

$$= -\frac{1}{\rho}\frac{\partial p}{\partial z} + G_z + f_z - b_z - \frac{R_{SOR}}{\rho V_F}(w - w_w - \delta w_s) \tag{4}$$

where (G_x, G_y, G_z) are body accelerations, (f_x, f_y, f_z) are viscous accelerations and (b_x, b_y, b_z) are flow losses in porous media or across porous baffle plates, and the final condition account for the injection of mass at a source represented by a geometry element (Manual, 2011).

Turbulence Model

In the current CFD simulation, Renormalization-group (RNG) turbulence model has been chosen considering for low Reynolds number effects (Koutsourakis *et al.,* 2012; A. Yakhot *et al.,* 1994; V. Yakhot & Orszag, 1986). Through applying the double averaging strategy to the transport equations for Turbulent Kinetic Energy (TKE) and its dissipation rate produces the turbulence model for the flow as displayed in Eqs. (5)-(8).

$$\frac{\delta k}{\delta t} + U_j\frac{\delta k}{\delta x_j} = \frac{\delta}{\delta x_j}\left[\left(v + \frac{v_t}{\sigma_k}\right)\frac{\delta k}{\delta x_j}\right] + P_k + B_k + W_k \tag{5}$$

$$\frac{\delta\varepsilon}{\delta t} + U_j\frac{\delta\varepsilon}{\delta x_j} = \frac{\delta}{\delta x_j}\left[\left(v + \frac{v_t}{\sigma_\varepsilon}\right)\frac{\delta\varepsilon}{\delta x_j}\right] + C_{1\varepsilon}\frac{\varepsilon}{k}(P_k + B_k)(1 + C_{3\varepsilon}R_f) + W_\varepsilon - C_{2\varepsilon}^*\frac{\varepsilon^2}{k} \tag{6}$$

$$P_k = v_tS^2 = v_t\left(\frac{\delta U_i}{\delta x_j} + \frac{\delta U_j}{\delta x_i}\right)\frac{\delta U_i}{\delta x_j} \tag{7}$$

$$B_k = \beta g_i\frac{v_t}{\sigma_s}\frac{\delta s}{\delta x_i} \tag{8}$$

where P_k is the shear production term of TKE, $S = \sqrt{2S_{ij}S_{ji}}$ is the average of strain tensor and $S_{ij} = \frac{1}{2}\left(\frac{\delta U_i}{\delta x_j} + \frac{\delta U_j}{\delta x_i}\right)$, B_k and W_k is the buoyant and wake production term of TKE, respectively. In addition, W_ε is the wake production term in ε, σ_k and σ_ε ae the turbulent Prandtl numbers for k and $\in$, and $C_{i\varepsilon}$, $C_{3\varepsilon}$ and $C_{2\varepsilon}^*$ are model coefficients.

Body Motion Equation

The body motion of the floating jetty is analyzed in the global coordinate system with reference to the geometry of the floating jetty. The motion

equations of motion of the rigid floating jetty are expressed in Eqs. (9)-(10) (Fitriadhy, Aldin, & Mansor, 2019):

$$\frac{d}{dt}(m\vec{v}_c) = \vec{f} \tag{9}$$

$$\frac{d}{dt}(M_c . \vec{w}_c) = \vec{m}_c \tag{10}$$

The index C shows the center of mass of the body, m is mass of the body, v_c the velocity vector, M_c is the tensor of the moments of inertia, w_c is the angular velocity vector and m_c represents the resultant moment vector acting on the body (Maki, Broglia, Doctors, & Di Mascio, 2013).

Waves

The Stokes wave theory is a nonlinear theory for limited amplitude progressive surface wave and can be generated at a mesh boundary. The wave theory implies that the fluid flow is incompressible and irrotational. The stream function occurs and satisfies the Laplace equation (see Eq. 11) (*Flow3D 10.1.1 User Manual*, 2013);

$$\nabla^2 \psi = 0 \tag{11}$$

Fluid velocity components in x and z are specified by Eqs. (12)-(13):

$$u = \frac{\partial \psi}{\partial x} \tag{12}$$

$$w = -\frac{\partial \psi}{\partial z} \tag{13}$$

The wave crest is assumed to exist at x=0 and t=0, the Laplace equation for was applied along the free surface and the bottom of boundary conditions to solve the computation via the perturbation method. The dimensionless wave amplitude, $\varepsilon = kH/2$ was used to compute the water velocity and elevation using Eqs. (14)-(16):

$$\eta(x,t) = d + \frac{\varepsilon}{k}\cos kX + \frac{\varepsilon^2}{k}B_{22}\cos 2kX + \frac{\varepsilon^3}{k}B_{31}(\cos kX - \cos 3kX)$$

$$+ \frac{\varepsilon^4}{k}B_{42}(\cos 2kX + B_{44}\cos 4kX) \tag{14}$$

$$+ \frac{\varepsilon^5}{k}[-(B_{53} + B_{55})\cos kX + B_{53}\cos 3kX + B_{55}\cos 5kX]$$

$$u(x,z,t) = U + C_0\left(\frac{g}{k^3}\right)^{V2}\sum_{i=1}^{5}\varepsilon^i\sum_{j=1}^{i}A_{ij}jk\cosh jkz \, \cos jkX \tag{15}$$

$$w(x,z,t) = C_0\left(\frac{g}{k^3}\right)^{V2}\sum_{i=1}^{5}\varepsilon^i\sum_{j=1}^{i}A_{ij}jk\sinh jkz \, \sin jkX \tag{16}$$

where $X = x - ct$, or $kX = kw -wt$. The coefficient A_{ij}, B_{ij}, C_0 and are nonlinear functions of and are described in Fenton (Fenton, 1985). The wave number and frequency are not independent parameters but satisfy the nonlinear equation as shown in Eq. (17):

$$\left(\frac{k}{g}\right)^{V2}U - \frac{\omega}{(gk)^{\frac{1}{2}}} + C_0 + \left(\frac{kH}{2}\right)^2 C_2 + \left(\frac{kH}{2}\right)^4 C_4 = 0 \tag{17}$$

where C_0, C_2 and C_4 are nonlinear functions of (Fenton, 1985).

Simulation Condition

Principal Data of Floating Jetty

The geometry of the floating jetty is shown in Figure 2, in which this floating jetty is made up composing of three main components i.e., floater, struts and deck, which is restrained by mooring-lines. The detailed particulars of the floating jetty are summarised in Table 1.
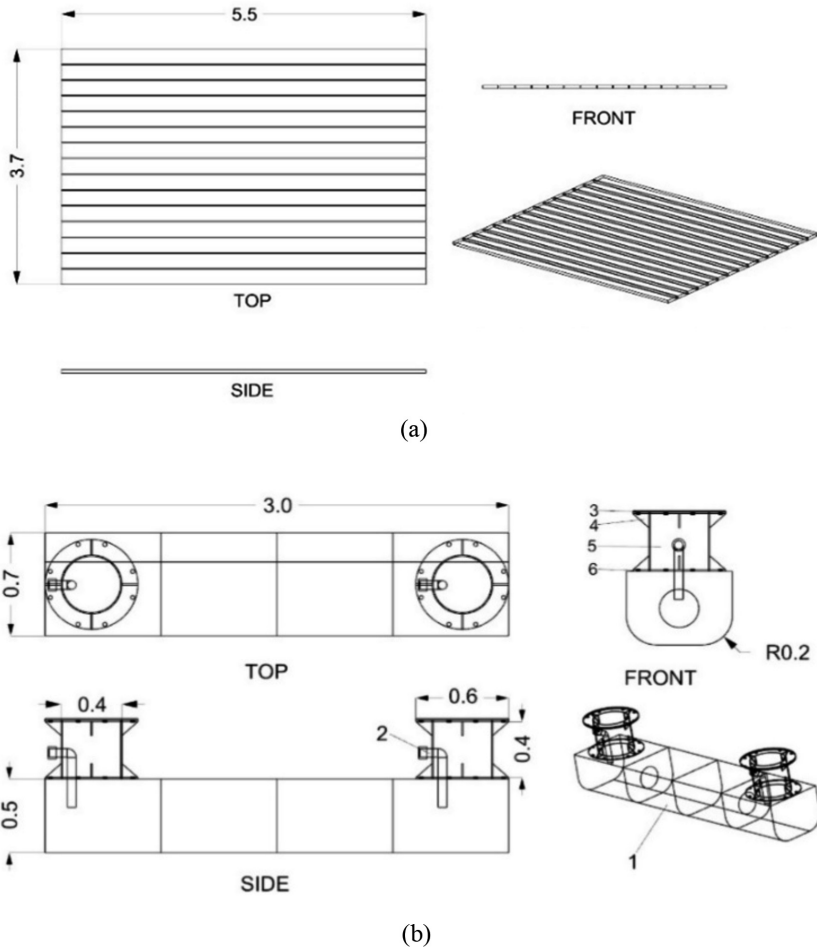
(a)

(b)

Figure 2: Floating jetty geometry consisting of; (a) deck structure and (b) pontoon structure

Table 1: Principle dimensions of floating jetty

Part	Quantity	Descriptions	Dimensions	Material
-	1	Deck	5.5 x 3.7 x 0.5 m	Wood
1	3	Pontoon	5.5 x 3.7 x 0.5 m	Fiberglass
2	6	Pipe	0.05 x 0.8 m	PVC
3	6	Plate Above	0.6 x 0.01 m	Fiberglass
4	24	Bracket	0.1 x 0.1 x 0.01 m	Fiberglass
5	6	Strut	0.4 x 0.4 m	Fiberglass
6	6	Plate Below	0.6 x 0.01 m	Fiberglass

Table 2: Matrix of computational fluid dynamics

H_w/L	Wavelength (λ/L)										
	0.50	0.75	1.00	1.25	1.50	1.75	2.00	2.25	2.50	2.75	3.00
0.045	√	√	√	√	√	√	√	√	√	√	√

Parametric Studies

The CFD simulations, were performed at various wavelengths from $\lambda/L=0.50$ to 3.00 as summarized in Table 2 and a wave height of $H_w/L= 0.045$ is assumed to be constant throughout.

Computational Domain and Boundary Conditions

The computational domain is presented as structured mesh and defined in Cartesian coordinates. Each of the boundary conditions as shown in the mesh block 1 and mesh block 2, is shown in Figure 3 (left). In mesh block 1, the boundary condition at X_{min} is defined as wave, while X_{max} is defined by outflow boundary to absorb the wave motion which will reduce the reflection from the boundary. Y_{min}, Y_{max} and Z_{min} are assigned as symmetrical boundaries which apply zero-gradient condition at the boundary and Z_{max} using specified pressure to create a uniform pressure at the boundaries. All mesh boundaries for mesh block 2 are defined by symmetry. The boundary conditions for the current CFD simulations are presented in Table 3.

The meshing generation is created in Flow-3D v11.2 as shown in Figure 3 (right). An extra refinement of the mesh called nested block is added to increase meshing resolution in this study. A full-scale floating jetty was assumed subjected to only three degrees of freedom (DOF) of motions i.e. surge, heave and pitch motions. The average duration for every simulation was about 70-80 hours.

Table 3: Boundary conditions

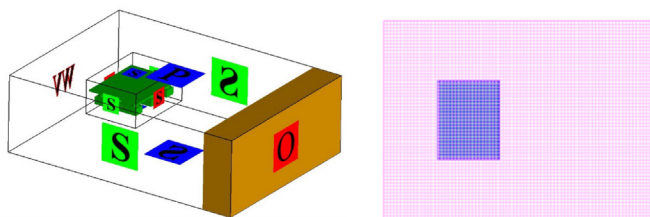| Boundary	Mesh block 1	Mesh block 2
	Wave	Symmetry
	Outflow	Symmetry
	Symmetry	Symmetry
	Symmetry	Symmetry
	Symmetry	Symmetry
	Specified pressure	Symmetry

Figure 3: Boundary conditions (left) and meshing generation (right)

Table 4: Mesh Independent study on floating jetty

Case	Total number of cells meshing	Heave motion, (m)	Pitch motion, (°)
A	1,281,312	0.01536	0.91651
B	1,789,200	0.01741	0.59806
C	2,530,188	0.01292	0.68079
D	3,133,464	0.01631	0.65278

In addition, a sufficient number of meshing are is very important in ensuring the stability of the computational results and reducing the CPU time. Consequently, four cases of the mesh independent study in different total number of cells meshing are successfully conducted (see Table 4). The total number of cells meshing of 2,530,188 was selected in all simulations of the floating jetty geometry with reasonable accuracy of the CFD solution. This indicates that the increase of total number of cells meshing up to 3,133,464 was unnecessary due to its insignificant effect on the computational results of the heave and pitch motions (A. Fitriadhy & Adam, 2017). The convergence result was analyzed by monitoring the residuals of continuity for heave and pitch motions responses. In fact, the optimum computed mesh numbers for the floating jetty were suitably chosen. In addition, a package software in Flow Sight was used to visualize the wave elevation for all various configurations of the floating jetty as shown in Figure 4.
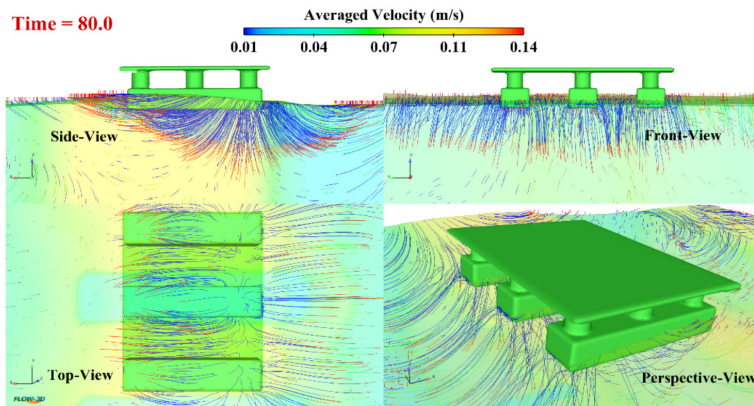

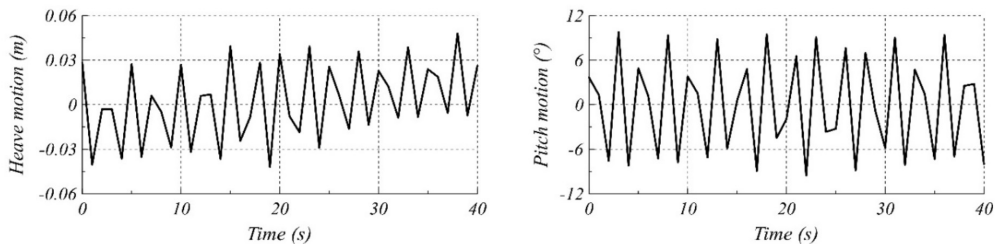Figure 4: Example view of floating jetty for case C

Figure 5: Time history for heave (left) and pitch (right) motions for case C

Results and Discussion

The CFD simulation of the full-scale of floating jetty model has been succesfully conducted, for $\lambda/L=0.50$ and t= 0 to 100 seconds (refer to Figure 6). Initially, the draft of the floating jetty was set at 70 cm (the waterline at the strust of the floating jetty). As the simulation time reached t=5 seconds, the draft was 40 cm (design draft). The floating jetty oscillated vertically, where the heave and pitch motions increased with respect to time.

Generally the simulation results, showed that the heave and pitch increases and decreases with increasing λ/L from 0.50 up to 3.00 with humps and hollows. The overall results are summarised in the Table 5. It is noted that the maximum heave motion response was 0.075 m at $\lambda/L= 2.75$.

The pitch motion showed a similar trend as in the heave motion but with much smoother response. The maximum pitch response was 20.06° at $\lambda/L= 2.25$. This possibly occurred due to the interaction between the structure (pontoon) and waves become relatively more stiff in RAO of the vertical motions as shown in Figure 8. It should be noted that the highest RAO of the heave and pitch motions are very important as it could result in loss of stability during operation and may cause an accident such as falling down into the sea (Siow *et al.,* 2015).

The heave and pitch motions decreased for the wavelengths from $\lambda/L= 1.75$ to 2.00 and 2.75 to 3.00 and from $\lambda/L= 2.25$ to 3.00, respectively. It is true that, the effects occurred due to the wavelength become larger than the
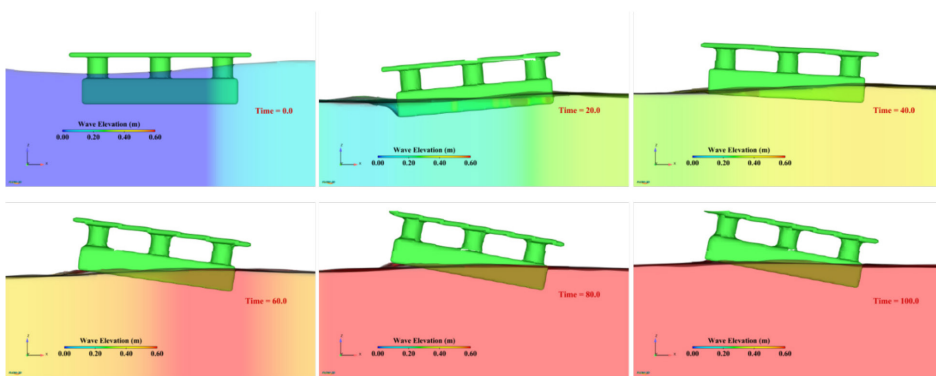

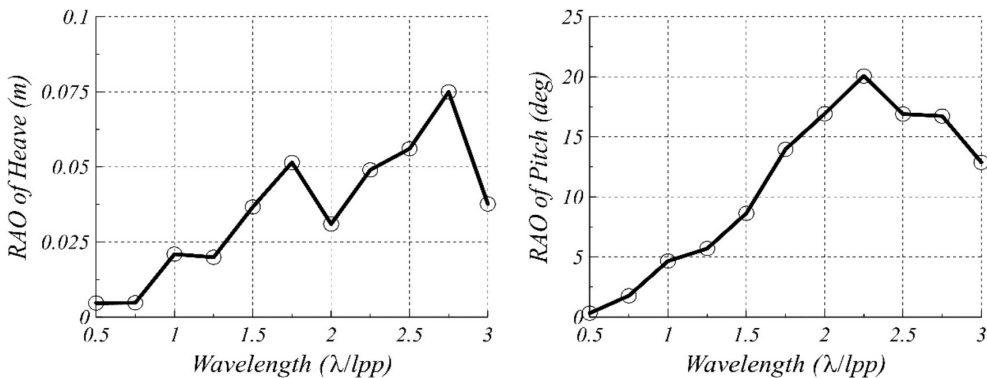Figure 6: 2D views of floating jetty at various time steps

Figure 7: Heave (left) and pitch (right) motions of floating jetty at various wavelengths with $H_w/L=0.045$ and $\theta= 0^0$

Table 5: Heave and pitch motions of floating jetty at various wavelengths (λ/L)

Ratios of λ/L	Heave motion (m)	Pitch motion (º)
0.50	0.0046	0.33
0.75	0.0048	1.77
1.00	0.0210	4.66
1.25	0.0199	5.70
1.50	0.0366	8.64
1.75	0.0515	13.96
2.00	0.0310	16.93
2.25	0.0490	20.06
2.50	0.0560	16.90
2.75	0.0750	16.72
3.00	0.0376	12.87

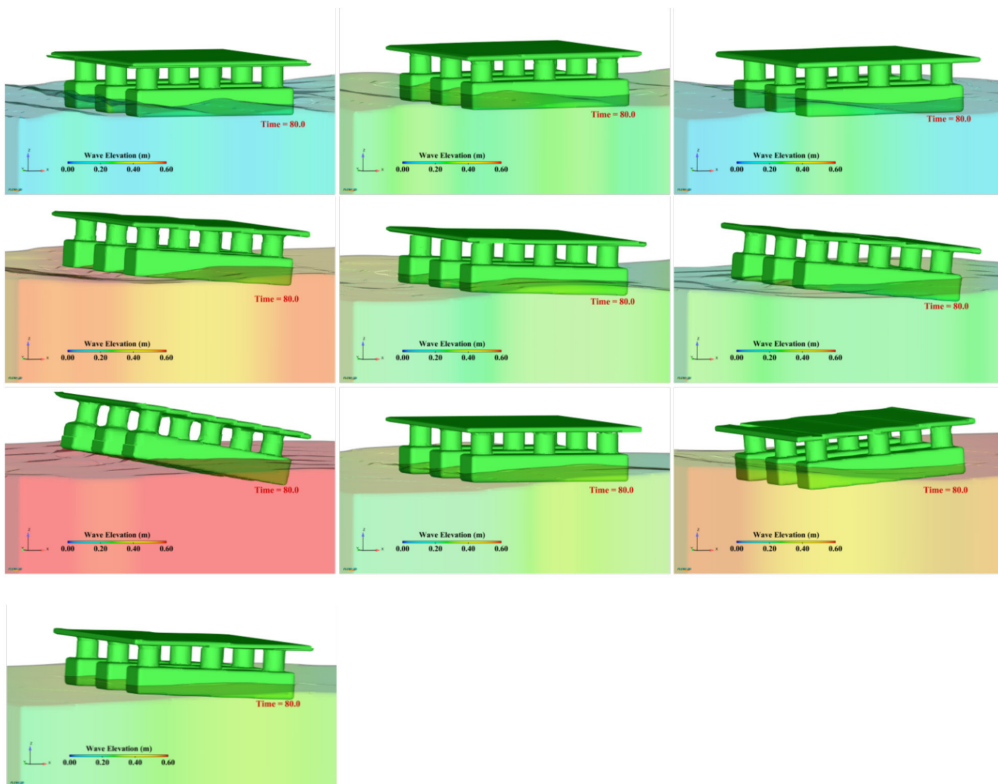Figure 8: Wave pattern characteristics of floating jetty at various wavelengths with H_w/L=0.045 and θ= 0º

length of floating jetty structure (A. Fitriadhy *et al.,* 2017). Therefore, it can be concluded that the floating jetty which is of a multi-hull configuration has relatively better vertical motion responses (heave and pitch motions) in short range of the wavelengths ($\lambda/L<2.25$).

Conclusion

Universiti Malaysia Terengganu has successfully designed and constructed a floating jetty as a landing infrastructure facility for the local fisherman community. The analysis of vertical motions of the full-scale floating jetty has been completely performed using CFD approach. The simulation results are then presented in the form of response amplitude motion i.e., heave and pitch motions. Several parameter studies such as effect of various wavelength in the range of $\lambda/L=$ 0.50 to 3.00 have been appropriately considered; where the results can be drawn as follows:

- The increase of wavelength from $\lambda/L=$ 0.50 to 2.25 produced insignificant vertical motions; which generally has a better stability during operation compared to other wavelength conditions.

- The subsequent increase of wavelength at $\lambda/L=$ 2.75, resulting in the highest heave motion of 0.0750 m; and the highest pitch motion achieved was 20.06° at $\lambda/L=$ 2.25.

Acknowledgements

References

Aribenchi, V. (2017). *Dynamics of Asymmetrical Configurations of Catamaran Hull Forms.*

Davis, M., & Holloway, D. (2007). A comparison of the motions of trimarans, catamarans and monohulls. *Australian Journal of Mechanical Engineering, 4*(2), 183-195.

Fenton, J. D. (1985). A fifth-order Stokes theory for steady waves. *Journal of Waterway, Port, Coastal, and Ocean Engineering, 111*(2), 216-234.

Fitriadhy, Aldin, N. A., & Mansor, N. A. (2019). CFD Analysis on course stability of a towed ship in calm water. *Journal of Sustainability Science and Management, 14*(4), 130-138.

Fitriadhy, A., & Adam, N. A. (2017). Heave and pitch motions performance of a monotricat ship in head-seas. *International Journal of Automotive and Mechanical Engineering, 14*, 4243-4258.

Fitriadhy, A., Faiz, M., & Abdullah, S. (2017). Computational fluid dynamics analysis of cylindrical floating breakwater towards reduction of sediment transport. *Journal of Mechanical Engineering and Sciences, 11*(4), 3072-3085.

Fitriadhy, A., Razali, N., & AqilahMansor, N. (2017). Seakeeping performance of a rounded hull catamaran in waves using CFD approach. *Journal of Mechanical Engineering and Sciences, 11*(2), 2601-2614.

Flow3D 10.1.1 User Manual. (2013). Flow Science Inc.

Grigoropoulos, G., Harries, S., Damala, D., Birk, L., & Heimann, J. (2003). *Seakeeping assessment for high-speed monohulls—A comparative study.* Paper presented at the 8th intl. marine design conf.

Kim, M., Hizir, O., Turan, O., & Incecik, A. (2017). Numerical studies on added resistance and motions of KVLCC2 in head seas for various ship speeds. *Ocean Engineering, 140*, 466-476.

Koutsourakis, N., Bartzis, J. G., & Markatos, N. C. (2012). Evaluation of Reynolds stress, k-ε and RNG k-ε turbulence models in street canyon flows using various experimental datasets. *Environmental fluid mechanics*, 1-25.

Luhulima, R. B., Setyawan, D., & Utama, I. (2014). *Selecting monohull, catamaran*

and trimaran as suitable passenger vessels based on stability and seakeeping criteria. Paper presented at the presenterd at The 14th International Ship Stability Workshop (ISSW), Kuala Lumpur, Malaysia, Sept.

Maki, K. J., Broglia, R., Doctors, L. J., & Di Mascio, A. (2013). Numerical investigation of the components of calm-water resistance of a surface-effect ship. *Ocean Engineering, 72*, 375-385.

Manual, F. D. U. (2011). Flow3D User Manual, v9. 4.2, Flow Science. *Inc., Santa Fe, NM*.

Siow, C., Koto, J., Yasukawa, H., Matsuda, A., Terada, D., Guedes Soares, C., & Samad MZbM, P. A. (2015). Wave induce motion of round shaped FPSO. *J Subsea Offshore*.

Yakhot, A., Rakib, S., & Flannery, W. (1994). Low-Reynolds number approximation for turbulent eddy viscosity. *Journal of scientific computing, 9*(3), 283-292.

Yakhot, V., & Orszag, S. A. (1986). Renormalization group analysis of turbulence. I. Basic theory. *Journal of scientific computing, 1*(1), 3-51.